PCCP

ROYAL SOCIETY OF CHEMISTRY

PAPER

View Article Online
View Journal | View Issue

Cite this: *Phys. Chem. Chem. Phys.*, 2025, **27**, 3817

Determination of the rotational isomerization rate along carbon–carbon single bonds in solution†

Seongchul Park,[ab] Hojeong Yoon,[b] Juhyang Shin[b] and Manho Lim *[b]

Received 24th November 2024,
Accepted 24th January 2025

DOI: 10.1039/d4cp04471a

rsc.li/pccp

The temperature- and viscosity-dependent rotational isomerization time constant (τ_{rot}) along the C–C$^{\bullet}$ bond of CF_2BrCF_2 radical in solution was measured using femtosecond infrared spectroscopy after photodissociating the I atom from CF_2BrCF_2I. Three density functional theory (DFT) functionals, ωB97XD, APFD, and B3LYP were used with the aug-cc-pVTZ basis set to calculate the required parameters in calculating τ_{rot} using Kramers' theory of reaction rates. The measured τ_{rot} was consistent with the value calculated using the vibrational frequencies and rotational barriers of the related compounds calculated by DFT method with ωB97XD/aug-cc-pVTZ. Kramers' theory calculation of τ_{rot} was further verified by an experimental measurement for $CF_3CF_2CF_2^{\bullet}$ in CCl_4 at 293 K. The τ_{rot} along the C–C(•) bond of ethyl radical and ethane derivatives in solution can be reliably estimated by Kramers' theory combined with DFT calculations using the ωB97XD functional and aug-cc-pVTZ basis set.

Introduction

Rotation along the C–C bond of a 1,2-disubstituted ethane derivative exchanges between relatively stable *gauche* and *anti* (*trans*) conformations, resulting in rotational isomers.[1,2] Rotational isomerization can influence the reactivity, dynamics, and biological activity of the related isomers.[3,4] Although the isomerization rate is an important factor describing reactions involving the isomer, it is rarely measured at room temperature because the rotation is ultrafast and difficult to measure. The rotational isomerization of a reaction intermediate, which may be more important for reactions involving the intermediate, is even harder to measure due to its short lifetime and fast rotation.[4]

The *anti–gauche* isomerization of *n*-butane is one of the simplest first-order chemical reactions and has thus been used as a model system for chemical reaction kinetics theory and molecular dynamics (MD) simulation studies of condensed phases.[5–10] Extensive theoretical studies reported that the isomerization time of *n*-butane in liquid is tens of picoseconds at room temperature.[5–10] However, no experimental confirmation of these theoretical results has been presented to date. Zheng *et al.* obtained the isomerization time of CH_2FCH_2NCO in CCl_4 at room temperature using 2D infrared (IR) vibrational echo spectroscopy.[3,4] Isomerization time constants of 40 (12) ps for *n*-butane (ethane) were estimated under the same conditions using the experimentally obtained values combined with the density functional theory (DFT) calculations of the barrier heights of the related compounds.[3,4] However, it was concluded that CH_2FCH_2NCO is not a good reference compound for estimating the rotational time of other ethyl derivatives because the calculations could not reproduce even the equilibrium isomer population of CH_2FCH_2NCO.[4]

Recently we measured the rotational isomerization time constant (τ_{rot}) of the C–C$^{\bullet}$ bond of CF_2BrCF_2 radical in CCl_4 solution at 280 K.[4] Excess *gauche* CF_2BrCF_2 radicals (*g*-$CF_2BrCF_2^{\bullet}$) were produced upon ultrafast dissociation of I atoms from the excited CF_2BrCF_2I in CCl_4 at 267 nm. The τ_{rot} was determined by probing that the excess *g*-$CF_2BrCF_2^{\bullet}$ isomerizes into *anti* CF_2BrCF_2 radicals (*a*-$CF_2BrCF_2^{\bullet}$) using the structure-specific femtosecond infrared spectroscopy. The barrier height of the rotation and the Gibbs free energies of two radical conformers, *g*-$CF_2BrCF_2^{\bullet}$ and *a*-$CF_2BrCF_2^{\bullet}$, were calculated using DFT. The calculated energies were then used to obtain the rotational time constants from *gauche* to *anti* (τ_{GA}) and *anti* to *gauche* (τ_{AG}), where $1/\tau_{rot} = 1/\tau_{GA} + 1/\tau_{AG}$. Based on the measured τ_{rot} and DFT calculations of ethyl radical derivatives and ethane derivatives (such as $CF_2BrCF_2^{\bullet}$, $CF_2ICF_2^{\bullet}$, $CH_3CH_2CH^{\bullet}CH_3$, $CH_3CH_2^{\bullet}$, CF_2BrCF_2I, CH_2FCH_2NCO, $CH_3CH_2CH_2CH_3$, and CH_3CH_3), the rotation time constants along the C–C(•) bond of these compounds were estimated under the same conditions. The time constant for the internal rotation was found to be similar to that calculated using transition state theory (TST) with a transmission coefficient (κ) of 0.75. However, it was not clear why $\kappa = 0.75$ was required and why the TST developed in the gas phase successfully estimated the

[a] *Korea Institute for Future Earth, Pusan National University, Busan 46241, Korea*
[b] *Department of Chemistry and Chemistry Institute for Functional Materials, Pusan National University, Busan 46241, Korea.*
E-mail: mhlim@pusan.ac.kr; Tel: +82 51 510 2243

† Electronic supplementary information (ESI) available. See DOI: https://doi.org/10.1039/d4cp04471a

rotational time in solution, where the compound is continuously perturbed by the interaction with solvent molecules.

The accuracy of the rotational energy barrier (E_{rot}) is critical to the accurate calculation of the rotational rate because the latter is proportional to $\exp(-E_{rot}/RT)$, where R and T are the gas constant and the absolute temperature, respectively. For example, the rotational rate changes by a factor of 2–0.5 at 298 K as E_{rot} changes $\pm$0.4 kcal mol^{-1}. Therefore, calculating accurate energy values for each conformer and the rotational barrier for a compound of interest is one of the most important factors in accurately calculating the rotation rate along the C–C($^{\bullet}$) bond of the compound using the rate equation. As E_{rot} can be experimentally estimated from the temperature-dependent rotational rates, the accuracy of the calculated E_{rot} values can be confirmed experimentally.

TST was developed by H. Eyring to describe reactions in the gas phase[11] based on the idea that the reaction proceeds at a rate at which an activated complex passes over the saddle point and assuming equilibrium between the reactants and activated complex.[12–14] For reactions in solution, the reactants are continuously disturbed by collisions with solvent molecules. Often, the solvent affects the chemical reaction by changing its potential energy surface (PES).[15] This effect is incorporated in TST by using the energies of the reactants and activated complex calculated in solution. Thus, solvent effects are incorporated to a certain degree in the rate constants estimated using the TST (k_{TST}) with energies calculated assuming a solution environment.[3,4] However, this approach excludes the dynamical solvent effects on the rate constant, which may impede or enhance molecular motion along the reaction coordinate.[12,13] Kramers showed that, based on the Langevin equation with a time-independent frictional coefficient, the dynamical solvent effect is represented by a transmission coefficient that depends on the ratio of the solvent friction and the curvature of the PES at the transition state (*i.e.*, Kramers' transmission coefficient, κ_{KR}) and the rate constant in solution, $k_s = \kappa_{KR} k_{TST}$.[13] The Kramers' theory of reaction rates was further developed using the generalized Langevin equation with a time-dependent solvent friction (Grote–Hynes theory).[16] Grote–Hynes theory is expressed as $k_s = \kappa_{GH} k_{TST}$, where κ_{GH} is a measure of the departure of the rate constant from k_{TST}. The calculation of κ_{GH} requires an MD simulation.[13]

In energy calculations of a target compound in solution, solvent effects were incorporated using the dielectric constant of the solvent as a parameter.[17] The polarity of the solvent, represented by the dielectric constant, is accounted for in the PES of the reaction in solution. Since the viscosity of the solvent represents the friction imposed on the reactant molecule along the reaction coordinate, it is a good parameter for the dynamical solvent effect. Measuring the reaction rates in solvents with various viscosities can reveal dynamical solvent effects that cannot be observed by measuring the rate in solvents with various dielectric constants. Thus, viscosity-dependent rotational time constants are considered useful in evaluating Kramer's theory of reaction rates to explicitly account for frictional forces imposed on the reaction coordinate by the solvent.

In this study, we measured the temperature- and the viscosity-dependent τ_{rot} of the C–C$^{\bullet}$ bonds of CF_2BrCF_2 radicals produced by immediate photodissociation of I atoms from CF_2BrCF_2I in CCl_4 solution using time-resolved IR (TRIR) spectroscopy. The energies of the reactants and activated complexes were calculated by DFT using three different functionals to identify a reliable and practical calculation method without using high-level calculations that require heavy computing power. The experimentally measured values were well reproduced by Kramers' theory with energies calculated by DFT using the ωB97XD functional and aug-cc-pVTZ basis set. These findings were further tested by measuring the τ_{rot} of the C–C$^{\bullet}$ bonds of $CF_3CF_2CF_2^{\bullet}$ after excitation of $CF_3CF_2CF_2I$ in CCl_4 at 293 K. The measured τ_{rot} of 34 ps is similar to the value of 30 ps calculated using Kramers' theory based on DFT calculations using ωB97XD/aug-cc-pVTZ.

Experimental details

Time-resolved mid-infrared spectroscopy

The femtosecond TRIR spectrometer used in this study was described in detail previously.[4,18,19] Briefly, a femtosecond pulse (800 nm, 110 fs, and 2 kHz) from a Ti:sapphire oscillator/amplifier system was split to pump an optical parametric amplifier (OPA) and a third harmonic generator (THG). The near-IR signal and idler pulses from the OPA were difference-frequency mixed by a GaSe crystal to generate tunable mid-IR pulses (120 fs and spectral width of 160 cm^{-1}). The THG produced a 120 fs, 267 nm pump pulse. A 1 μJ UV pulse was optically advanced relative to the mid-IR probe pulse and used to excite the sample, which was probed by the weak ($\sim$10 nJ) mid-IR probe pulse. The isotropic absorbance was measured by setting the relative polarization of the pump pulse to that of the probe pulse magic angle (54.7°). The experiment was repeated with probe pulses centered at 920 or 940 cm^{-1} for CF_2BrCF_2 and 1050, 1130, 1210, 1270, or 1330 cm^{-1} for $CF_3CF_2CF_2^{\bullet}$. The data were combined for broader spectral regions than the spectral width of the probe pulses (160 cm^{-1}). The probe pulses were sent through the sample and detected by 1 × 128 or 1 × 64 pixel MCT array detectors for wavenumbers of $>$1000 and $<$1000 cm^{-1}, respectively, with a 320 mm monochromator with a grating of 50, 75, or 100-lines per mm. These settings resulted in a spectral resolution of 1 and 2.7 cm^{-1} for the spectral regions of $>$1000 and $<$1000 cm^{-1}, respectively. The instrument response function was 0.2 ps. To avoid complication arising from the overlap of pump and probe pulses, data were collected starting from 0.3 ps.

Sample preparation

CF_2BrCF_2I and *n*-hexane were purchased from Alfa Aesar and $CF_3CF_2CF_2I$, CCl_4, and DMF were purchased from Sigma-Aldrich and used without further purification. The flowing sample cell consisted of two 2-mm-thick BaF_2 windows and a 100-μm-thick Teflon spacer. A peristaltic tubing pump was used to refresh 50 mM CF_2BrCF_2I or $CF_3CF_2CF_2I$ in the sample cell fast enough for each probe pulse at a repetition rate of 2 kHz.

The sample volume was sufficiently large to maintain the sample concentration above 98% of the initial concentration, even after the photoreaction of the sample by 267-nm excitation. The temperature of the sample was adjusted by passing a coolant through the sample mount block, which maintained the temperature within ±2 K of the set value. Equilibrium UV-vis and FTIR spectra were collected throughout the experiment to ensure the integrity of the sample.

Computational details

All quantum chemical calculations were performed using Gaussian 16 software.[20,21] The DFT method with three different functionals (ωB97XD,[22,23] APFD,[24] and B3LYP[25]) and the aug-cc-pVTZ basis set was used for molecular geometry optimization and calculating the vibrational frequency and energies of the optimized compounds. The ωB97XD functional (the long-range corrected hybrid density functional with damped atom–atom dispersion corrections) has been reported to yield satisfactory accuracy for thermochemistry, kinetics, and non-covalent interactions.[22–27] The APFD functional (the Austin–Frisch–Petersson functional with dispersion) was reported to reproduce the relative conformational energies of organic molecules and the accuracy of weak interactions is comparable to that of CCSD(T)/aug-cc-pVTZ.[24] The B3LYP functional (the Becke, 3-parameter, Lee–Yang–Parr exchange–correlation functional) is one of the most commonly used hybrid functionals.[25] The solvent effects were incorporated into the polarizable continuum model using the integral equation formalism variant. The calculated parameters were used to calculate the rotational rate constant of an interested compounds using Kramers' theory of reaction rates.

Results and discussion

Fig. 1 displays IR spectra of CF_2BrCF_2I, *a*-$CF_2BrCF_2^\bullet$, and *g*-$CF_2BrCF_2^\bullet$ in CCl_4. The equilibrium FTIR spectrum of CF_2BrCF_2I was collected at room temperature. The spectra of the two radicals were obtained from the previous study on the photodissociation dynamics of CF_2BrCF_2I in CCl_4 at 267 nm.[4] Although most of the spectral features of three compounds overlap in the 1400–1050 cm^{-1} range, the absorption bands in the 1050–850 cm^{-1} range are significantly different for each compound, enabling these bands to be readily distinguished. Therefore, population changes of the three compounds over time can be easily monitored by observing changes in the 1050–850 cm^{-1} range of the TRIR spectra.

TRIR spectra of CF_2BrCF_2I in CCl_4 at 280, 300, and 310 K were collected in the spectral region of 1050–850 cm^{-1} from 0.3 to 1000 ps after excitation at 267 nm and representative TRIR spectra are shown in Fig. 2(a). The negative band at 993 cm^{-1} arises from the population depletion of CF_2BrCF_2I as I atoms are immediately dissociated upon excitation at 267 nm. The magnitude of this band remained stable over the measurement period, implying that no geminate recombination (GR) of the dissociated pairs within 1 ns. The magnitudes of the two absorption bands near 900 cm^{-1} changed over

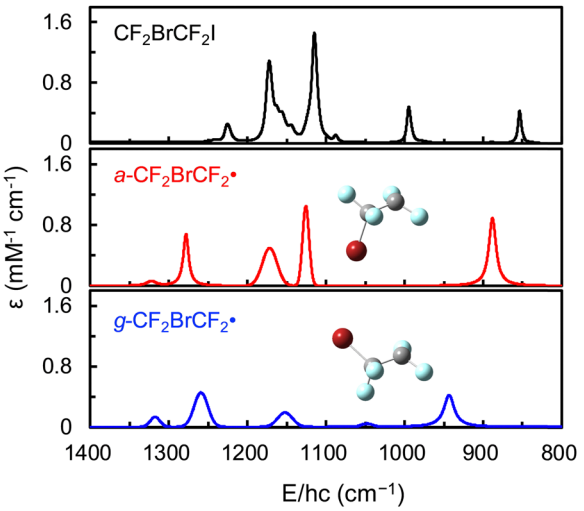

Fig. 1 IR spectra of CF_2BrCF_2I, *a*-$CF_2BrCF_2^\bullet$, and *g*-$CF_2BrCF_2^\bullet$ in CCl_4 solution. Inset: Optimized structures of two CF_2BrCF_2 radicals calculated using DFT method employing ωB97XD/aug-cc-pVTZ. The gray, light blue, and red spheres represent C, F, and Br atoms, respectively.

time, accompanied by peak narrowing and blue shifts. The blue-shifted and narrowed bands at 943 and 888 cm^{-1} arise from *g*-$CF_2BrCF_2^\bullet$ and *a*-$CF_2BrCF_2^\bullet$, respectively. The spectral narrowing and blue shifts result from the thermalization of the nascent radicals produced under excess energy with a time constant of 15 ± 3 ps.[4] The decay of the 943 cm^{-1} band and simultaneous intensification of the 888 cm^{-1} band result from the equilibration of excess *g*-$CF_2BrCF_2^\bullet$ produced during the photodissociation of CF_2BrCF_2I *via* the rotational isomerization of the nascent radicals.[4] The population of each compound was obtained from the amplitude of the corresponding band once its extinction coefficient was determined. The relative integrated extinction coefficient of the band at 943 cm^{-1} compared with that at 888 cm^{-1}, estimated from the spectra shown in Fig. 1, is 0.57 ± 0.03. Fig. 3(a) exhibits the changes in the mole fractions of *a*-$CF_2BrCF_2^\bullet$ and *g*-$CF_2BrCF_2^\bullet$ over time, which were determined from the changes in the integrated area of the corresponding bands and the ratio of the integrated extinction coefficients of the bands. As shown in Fig. 3(a), the changes in mole fractions at 280, 300, and 310 K were well described by the interconversion kinetics between two isomers, with time constants of 48, 34, and 30 ps, respectively. These values represent the τ_{rot} for the C–C$^\bullet$ bond of $CF_2BrCF_2^\bullet$ in CCl_4 at the corresponding temperatures.

The excess energy from the photodissociation of vicinal dihaloethanes has been reported to partition roughly equally between internal degrees of freedom and translation.[28,29] Given that the excitation energy is 107 kcal mol^{-1} (267 nm) and the dissociation energy of the C–I bond is 52 kcal mol^{-1}, the internal energy of the nascent $CF_2BrCF_2^\bullet$ is approximately 28 kcal mol^{-1}. The partitioning between rotational and vibrational energies remains unknown. Clearly, the dissociation of $CF_2BrCF_2^\bullet$ would generate considerable rotational energy, but this excess energy is expected to relax into the surrounding

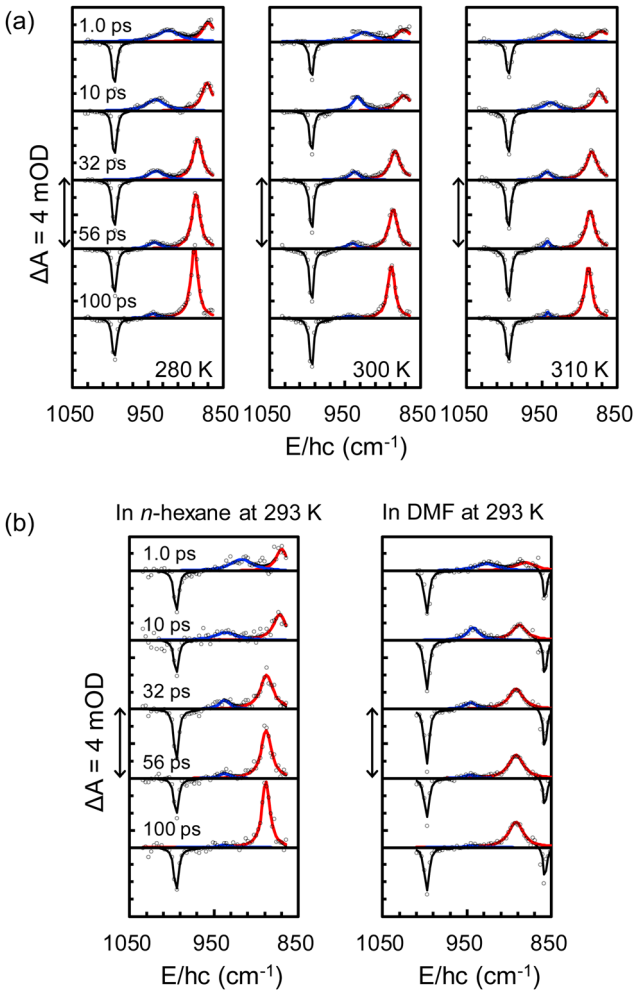

Fig. 2 Representative TRIR spectra of CF_2BrCF_2I in (a) CCl_4 at 280, 300, and 310 K and in (b) *n*-hexane and DMF at 293 K collected 0.3–1000 ps after excitation at 267 nm in the spectral region of 1050–850 cm^{-1} where absorption bands for reactant and photoproducts are well separated. The absorbance difference (ΔA) is given in units of optical density (OD), where 1 mOD = 10^{-3} OD. Data (open circles) are well reproduced by summing the three absorption bands for CF_2BrCF_2I (black), *g*-$CF_2BrCF_2^\bullet$ (blue), and *a*-$CF_2BrCF_2^\bullet$ (red). A bleach band appears near 850 cm^{-1} in DMF as the band shifts within the probe window. This band is outside the probe window in other solvents.

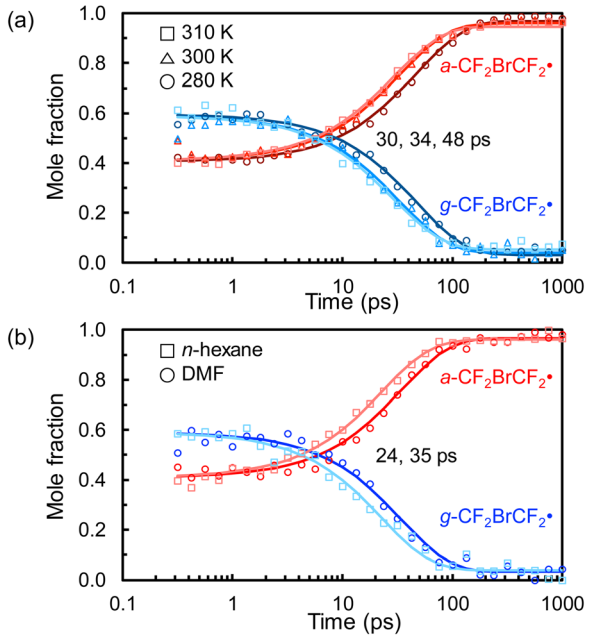

Fig. 3 (a) Changes of the mole fractions for *g*-$CF_2BrCF_2^\bullet$ and *a*-$CF_2BrCF_2^\bullet$ produced by the photoexcitation of CF_2BrCF_2I in CCl_4 at 280, 300, and 310 K. Excess *g*-$CF_2BrCF_2^\bullet$ was produced upon photoexcitation at 267 nm and relaxes to equilibrium mole fractions of 0.02–0.03, 0.02–0.04, and 0.03–0.05 at 280, 300, and 310 K, respectively. The equilibrium mole fraction was estimated from the calculated Gibbs free energy differences between two $CF_2BrCF_2^\bullet$ isomers in CCl_4 at 280, 300, and 310 K using DFT with the aug-cc-pVTZ basis set (Table 1). The changes in the mole fractions (symbols) were well described by the interconversion kinetics between two isomers (solid lines) with time constants of 48, 34, and 30 ps, which are attributed to the τ_{rot} values for the C–C$^\bullet$ bond of $CF_2BrCF_2^\bullet$ in CCl_4 at 280, 300, and 310 K, respectively. (b) Changes in the mole fractions of *g*-$CF_2BrCF_2^\bullet$ and *a*-$CF_2BrCF_2^\bullet$ under the photoexcitation of CF_2BrCF_2I in *n*-hexane and DMF at 293 K. Excess *g*-$CF_2BrCF_2^\bullet$ was produced upon photoexcitation at 267 nm, which relaxes to an equilibrium fraction of 0.02–0.04. This was estimated from the calculated Gibbs free energy differences between two $CF_2BrCF_2^\bullet$ isomers in *n*-hexane and DMF at 293 K using DFT with the aug-cc-pVTZ basis set (Table 1). The changes in the mole fractions (symbols) were well described by the interconversion kinetics between two isomers (solid lines) with time constants of 24 and 35 ps, which are attributed to the τ_{rot} values of the C–C$^\bullet$ bond of $CF_2BrCF_2^\bullet$ in *n*-hexane and DMF at 293 K, respectively. The nascent photoproducts of CF_2BrCF_2I at 267 nm are ~18% $CF_2ICF_2^\bullet$ and ~82% $CF_2BrCF_2^\bullet$, but we considered only $CF_2BrCF_2^\bullet$ in calculating the mole fractions for simplicity.

solvent within a few picoseconds. Thus, the rotational isomerization process is unlikely to be significantly affected by the excess energy. The dissociated I atom may remain in the vicinity of $CF_2BrCF_2^\bullet$. Due to its bulkiness and polarizability, the presence of the I atom could influence the dielectric environment and mechanical friction of the C–C isomerization process, as well as the Gibbs free energy of the nascent radical. If the I atom remains near the nascent CF_2BrCF_2 radical, it could geminately rebind with the radical, reverting it to the reactant. However, no GR was observed in the photodissociation of CF_2BrCF_2I at 267 nm,[19] indicating that the dissociated I atom does not stay close enough to interact with $CF_2BrCF_2^\bullet$. Therefore, the presence of the dissociated I atom was not considered in the analysis of the C–C isomerization process. While the excess rotational and translational energies of radicals produced from photodissociation dissipate within a few picoseconds, the excess vibrational energy relaxes on the same time scale as the observed rotational isomerization time constants. Although the impact of excess vibrational energy on rotational isomerization remains unclear, it may accelerate the process. Therefore, the experimentally observed rotational time constants represent the lower limit.

As mentioned above, a solvent can influence a chemical reaction by perturbing the reaction PES. The energies of the reactants and activated complex in solution were calculated by incorporating the dielectric constant of the solvent to represent its contribution.[30] To explore the contribution of the solvent viscosity (dynamical solvent effect), comparative measurements

Table 1 Change in the Gibbs free energy of g-$CF_2BrCF_2^\bullet$ relative to a-$CF_2BrCF_2^\bullet$ (ΔG) and the mole fraction of g-$CF_2BrCF_2^\bullet$ (x_G) in various solvents at various temperatures. The energies were calculated at the given temperatures using three different DFT functionals (ωB97XD, APFD, and B3LYP) and the aug-cc-pVTZ basis set

Solvent	Method	Temp. (K)	ΔG (kcal mol^{-1})	x_G (%)
CCl_4	ωB97XD	280	2.258	3.3
		293	2.253	4.0
		300	2.251	4.4
		310	2.247	5.0
	APFD	280	2.586	1.9
		293	2.581	2.3
		300	2.578	2.6
		310	2.573	3.0
	B3LYP	280	2.668	1.6
		293	2.664	2.0
		300	2.663	2.3
		310	2.659	2.6
n-Hexane	ωB97XD	293	2.257	4.0
	APFD		2.583	2.3
	B3LYP		2.668	2.0
DMF	ωB97XD	293	2.224	4.2
	APFD		2.560	2.4
	B3LYP		2.632	2.1

of the reaction rates using solvents with different viscosities but the same dielectric constants or the same viscosities but different dielectric constants would be valuable. A good solvent for TRIR spectroscopy under 267-nm excitation should have negligible absorption at 267 nm, a good IR spectral window in the probed spectral region (here, 1050–850 cm^{-1}), and reasonable solubility of the target reactant molecule. *n*-Hexane and dimethylformamide (DMF) are good solvents for the TRIR spectroscopy of CF_2BrCF_2I as they satisfy the above-mentioned conditions. In addition, the dielectric constant (ε) of *n*-hexane (ε = 1.882) is similar to that of CCl_4 (ε = 2.228) but its viscosity (0.31 mPa s at 293 K) is about one-third that of CCl_4 (0.91 mPa s at 293 K).[31] In contrast, the viscosity of DMF (0.86 mPa s at 293 K) is similar to that of CCl_4, but its dielectric constant (ε = 37.32) is about 17 times higher than that of CCl_4. Therefore, the τ_{rot} values of $CF_2BrCF_2^\bullet$ were also measured in *n*-hexane and DMF solutions for comparison.

TRIR spectra of CF_2BrCF_2I in *n*-hexane and DMF were collected at 293 K in the spectral region of 1050–850 cm^{-1} from 0.3 to 1000 ps after excitation at 267 nm. Representative TRIR spectra are shown in Fig. 2(b). The bleach bands arise from the population depletion of CF_2BrCF_2I and their magnitudes remain constant up to 1 ns, as is the case for the TRIR spectra of CF_2BrCF_2I in CCl_4. Although the absorption bands in *n*-hexane and DMF are slightly shifted compared to those obtained in CCl_4, the spectral evolution is similar to that observed in CCl_4, namely the decay of the band near 940 cm^{-1} and simultaneous growth of the band near 890 cm^{-1}, accompanied by blue shifts and peak narrowing. Therefore, the bands near 940 and 890 cm^{-1} were assigned to g-$CF_2BrCF_2^\bullet$ and a-$CF_2BrCF_2^\bullet$, respectively.

The changes in the mole fractions of g-$CF_2BrCF_2^\bullet$ and a-$CF_2BrCF_2^\bullet$ in *n*-hexane and DMF were obtained from the time-dependent amplitude changes of the corresponding bands by assuming that their integrated extinction coefficients are the same as those in CCl_4. Inaccuracies in the extinction coefficients result in changes in the final equilibrated mole fractions but they do not influence the τ_{rot} values, which are the parameters of interest here. As shown in Fig. 3(b), the mole fractions of g-$CF_2BrCF_2^\bullet$ and a-$CF_2BrCF_2^\bullet$ in *n*-hexane and DMF at 293 K change simultaneously, and τ_{rot} values of 24 and 35 ps, respectively, were determined.

A τ_{rot} of 37 ps for $CF_2BrCF_2^\bullet$ in CCl_4 at 293 K was interpolated from data at 280, 300, and 310 K. Changing the solvent from CCl_4 to *n*-hexane results in a decrease in the viscosity (by a factor of $\sim$3), and the corresponding τ_{rot} decreases by $\sim$1.5 times. In contrast, the significant difference in the dielectric constants (that of DMF is $\sim$17 times higher than that of CCl_4) has a negligible effect on τ_{rot}. Therefore, the τ_{rot} of $CF_2BrCF_2^\bullet$ is significantly affected by the solvent viscosity but not its dielectric constant. When the charge distribution of the reactant is similar to that in the transition state and/or the polarities of the reactant compounds are small, the PES along the reaction coordinate is not significantly influenced by the polarity of the solvent (*i.e.*, the dielectric constant), and thus has little influence on the rate constant of the reaction.[12,13]

Kramers expressed the rate constant of a chemical reaction in solution, k_s, as follows:[12,13]

$$k_s = \frac{\omega_R}{2\pi\omega_{TS}}\left(\sqrt{\frac{\gamma^2}{4}+\omega_{TS}{}^2}-\frac{\gamma}{2}\right)\exp\left(-\frac{\Delta_r E}{RT}\right) \quad (1)$$

where $\gamma = \frac{6\pi\eta R_h}{M}$, $\Delta_r E = E_{TS} - E_R$.

Here, ω_{TS} and ω_R are the angular frequencies associated with the reactive mode in the transition state and reactant, respectively, γ is the friction constant of the solvent, M is the reactant mass, η is the viscosity of the solvent, R_h is the hydrodynamic radius of the compound, and E_{TS} and E_R are the energies of the transition state and reactant, respectively. Eqn (1) can be further expressed as follows:[13]

$$k_s = \frac{1}{\omega_{TS}}\left(\sqrt{\frac{\gamma^2}{4}+\omega_{TS}{}^2}-\frac{\gamma}{2}\right)\times\frac{\omega_R}{2\pi}\exp\left(-\frac{\Delta_r E}{RT}\right) \quad (2)$$

$$k_s = \kappa_{KR} k_{TST}$$

where

$$\kappa_{KR} = \sqrt{1+\left(\frac{\gamma}{2\omega_{TS}}\right)^2}-\frac{\gamma}{2\omega_{TS}}$$

$$k_{TST} = \frac{\omega_R}{2\pi}\exp\left(-\frac{\Delta_r E}{RT}\right)$$

Kramers' theory of reaction rates shows that k_s is described simply as a product of the transmission coefficient, κ_{KR}, and the rate constant calculated by conventional TST, k_{TST}. In Kramers' theory, the dynamical solvent effect is represented

by κ_{KR}. As E_{TS} and E_R are calculated in solution, the static solvent effect is incorporated in k_{TST} *via* $\Delta_r E$.

The rotational interconversion rates for the *anti*-to-*gauche* (k_{AG}) and *gauche*-to-*anti* (k_{GA}) conversions of $CF_2BrCF_2^\bullet$ were calculated using Kramers' theory with the corresponding k_{TST} ($k_{TST,AG}$ and $k_{TST,GA}$, respectively) and κ_{KR} (κ_{KR}^A, κ_{KR}^G, respectively) values as follows.

$$\begin{aligned} k_{AG} &= \kappa_{KR}^A k_{TST,AG} \\ k_{GA} &= \kappa_{KR}^G k_{TST,GA} \end{aligned} \quad (3)$$

where

$$k_{TST,AG} = 2\frac{\omega_A}{2\pi}\exp\left(-\frac{\Delta E_{TA}}{RT}\right), \quad \Delta E_{TA} = E_{TS} - E_A$$

$$k_{TST,GA} = \frac{\omega_G}{2\pi}\exp\left(-\frac{\Delta E_{TG}}{RT}\right), \quad \Delta E_{TG} = E_{TS} - E_G$$

$$\kappa_{KR}^A = \sqrt{1 + \left(\frac{\gamma^A}{2\omega_{TS}}\right)^2} - \frac{\gamma^A}{2\omega_{TS}}, \quad \gamma^A = \frac{6\pi\eta R_h^A}{M}$$

$$\kappa_{KR}^G = \sqrt{1 + \left(\frac{\gamma^G}{2\omega_{TS}}\right)^2} - \frac{\gamma^G}{2\omega_{TS}}, \quad \gamma^G = \frac{6\pi\eta R_h^G}{M}$$

Here, ω and E have the same meanings as in eqn (1), and the subscripts or superscripts *G* and *A* indicate the *gauche*- and *anti*-states of the isomer, respectively. R_h^A and R_h^G represent the hydrodynamic radii of the *anti* and *gauche* compounds, respectively. Note that multiplication by the pre-factor of 2 is required in the calculation of $k_{TST,AG}$ as there are two *gauche* isomers in $CF_2BrCF_2^\bullet$.[4] The rotational isomerization rate, k_{rot} is obtained from the rotational interconversion rates:[4]

$$k_{rot} = k_{AG} + k_{GA} \quad (4)$$

Therefore, τ_{rot} is calculated using

$$\tau_{rot} = \frac{1}{k_{AG} + k_{GA}} \quad (5)$$

Three different DFT functionals were used to calculate the energies and vibrational frequencies of the target compounds using the aug-cc-pVTZ basis set. Namely, ωB97XD was reported to yield satisfactory accuracy in thermochemical studies,[22,23] APFD is reliable for energy calculations,[24,26] and B3LYP is one of the most widely used DFT methods.[25,27] Table 2 shows the τ_{rot} values of $CF_2BrCF_2^\bullet$ dissolved in various solvents obtained using Kramers' theory based on the energies and vibrational frequencies calculated using the three DFT functionals. Among the values calculated using the three DFT functionals, although the κ_{KR} values are similar and the rotational barriers are within a fraction of a kcal mol^{-1}, the τ_{rot} values significantly differ. The ΔE_{TG} of $CF_2BrCF_2^\bullet$ in CCl_4 is smaller than ΔE_{TA} by 2.32–2.74 kcal mol^{-1}, resulting in a k_{GA} that is more than 18 times larger than k_{AG}. Therefore, the τ_{rot} of $CF_2BrCF_2^\bullet$ is dominated by the interconversion time of $(k_{GA})^{-1}$, implying that ΔE_{TG} is the major influencing factor in the calculation of τ_{rot}. The ΔE_{TG} values calculated using the three DFT functionals differ marginally, by <0.36 kcal mol^{-1}, which is within the accepted accuracy of energy calculations for general purposes. However, the

Table 2 Rotational isomerization time constant calculated using the Kramers' theory ($\tau_{rot}^{(cal'd)}$) for $CF_2BrCF_2^\bullet$ dissolved in various solvents. The experimentally determined values ($\tau_{rot}^{(exp)}$) are shown for the comparison. Energies and vibrational frequencies were calculated using three different DFT functionals (ωB97XD, APFD, and B3LYP) and the aug-cc-pVTZ basis set. Zero-point corrected energies were used to calculate the rotational energy barrier. The reactive mode in the transition state (ω_{TS}) corresponds to the mode with an imaginary frequency in the transition sate

Solvent[31]	Method	Temp. (K)	Viscosity[32,33] (mPa s)	$\frac{\omega_{TS}}{2\pi c}, \frac{\omega_A}{2\pi c}, \frac{\omega_G}{2\pi c}$ (cm^{-1})	ΔE_{TG} (kcal mol^{-1})	ΔE_{TA} (kcal mol^{-1})	κ_{KR}^A, κ_{KR}^G	$\tau_{rot}^{(cal'd)}$ (ps)	$\tau_{rot}^{(exp)}$ (ps)
CCl_4 (ε = 2.228)	ωB97XD	280	1.13	65, 72, 59	2.06	4.40	0.42, 0.38	58	48
		293	0.91				0.48, 0.44	42	(37)[a]
		300	0.83				0.51, 0.47	36	34
		310	0.72				0.55, 0.51	30	30
	APFD	280	1.13	63, 70, 57	1.70	4.38	0.36, 0.37	33	48
		293	0.91				0.42, 0.43	25	—
		300	0.83				0.45, 0.46	21	34
		310	0.72				0.49, 0.50	18	30
	B3LYP	280	1.13	64, 71, 57	1.87	4.61	0.41, 0.40	44	48
		293	0.91				0.47, 0.46	30	—
		300	0.83				0.50, 0.50	26	34
		310	0.72				0.54, 0.54	22	30
n-Hexane (ε = 1.882)	ωB97XD			66, 72, 59	2.08	4.42	0.73, 0.74	26	23
	APFD	293	0.31	64, 71, 57	1.73	4.40	0.74, 0.74	15	23
	B3LYP			64, 71, 56	1.89	4.63	0.74, 0.72	20	23
DMF (ε = 37.22)	ωB97XD			64, 72, 58	1.92	4.24	0.48, 0.46	32	35
	APFD	293	0.86	60, 70, 55	1.57	4.23	0.44. 0.47	19	35
	B3LYP			61, 71, 56	1.72	4.43	0.45, 0.44	25	35

[a] Interpolated value from data at 280, 300, and 310 K.

calculated τ_{rot} values for $CF_2BrCF_2^\bullet$ in CCl_4 differ by up to 1.9 times (see Table 2). As stated earlier, accurate PES values are a prerequisite for accurately calculating rate constants. Although high-level calculations of the PES along the reaction coordinate would be beneficial for the accurate calculation of the rate constants, DFT calculations were used for the sake of practicality, as high-level methods such as CCSD(T) require more time and computing power.

As expected, the κ_{KR} values were similar for solvents with similar viscosities, such as CCl_4 and DMF. Although the dielectric constant of DMF is 17 times larger than that of CCl_4, the rotational energy barriers of $CF_2BrCF_2^\bullet$ in these two solvents differ by only 0.13–0.18 kcal mol^{-1}, resulting in similar τ_{rot} values in these solvents, *i.e.*, 42 (32), 25 (19), and 30 (25) ps in CCl_4 (DMF) at 293 K were calculated using the ωB97XD, APFD, and B3LYP functionals, respectively. The κ_{KR} of $CF_2BrCF_2^\bullet$ in *n*-hexane is 1.6–1.7 times larger than that in CCl_4, but the rotational energy barriers are similar in *n*-hexane and CCl_4, resulting in smaller τ_{rot} values in *n*-hexane (by a factor of 1.5–1.7). The rotational isomerization of $CF_2BrCF_2^\bullet$ in *n*-hexane was ∼1.6 times faster than that in CCl_4 due to the 3 times smaller viscosity of *n*-hexane than CCl_4, resulting in 1.6–1.7 times larger κ_{KR} values. The influence of solvent viscosity on C–C$^\bullet$ bond rotation is significant whereas that of the solvent dielectric constant is negligible, and Kramers' theory successfully estimated τ_{rot} of the C–C$^\bullet$ bond for $CF_2BrCF_2^\bullet$ in solution.

Table 2 shows the temperature-dependent τ_{rot} values of the C–C$^\bullet$ bond for $CF_2BrCF_2^\bullet$ in CCl_4 and the viscosity-dependent τ_{rot} values at 293 K calculated based on the energies and vibrational frequencies of the related compounds using three-different DFT functionals. The experimentally determined τ_{rot} values of $CF_2BrCF_2^\bullet$ in CCl_4 at 280, 300, and 310 K, as well as those in *n*-hexane and DMF, best match the values obtained based on the DFT calculation using ωB97XD/aug-cc-pVTZ. Although the ωB97XD functional provided the best match with the experimental values, the other functionals used (APFD and B3LYP) also resulted in a reasonable match.

To test the validity of the rate constants calculated by Kramers' theory, we measured the τ_{rot} about the C–C$^\bullet$ bond of ethyl derivatives other than $CF_2BrCF_2^\bullet$ and compared the values with the calculated ones. The equilibrium UV-vis and FTIR spectra of $CF_3CF_2CF_2I$ are given in Fig. 4. This compound is known to dissociate I atoms upon UV excitation[34] and the produced radicals are expected to have two rotational conformers, *g*-$CF_3CF_2CF_2^\bullet$ and *a*-$CF_3CF_2CF_2^\bullet$. TRIR spectra of $CF_3CF_2CF_2I$ in CCl_4 at 293 K were collected from 0.3 to 1000 ps in the spectral region of 1400–1000 cm^{-1} after excitation at 267 nm and representative TRIR spectra are shown in the lower panel of Fig. 5. Although congested, the TRIR spectra were expected to include contributions from three compounds: the reactant ($CF_3CF_2CF_2I$) and two photoproducts (*g*-$CF_3CF_2CF_2^\bullet$ and *a*-$CF_3CF_2CF_2^\bullet$). The TRIR spectra were globally fitted using three basis spectra: equilibrium $CF_3CF_2CF_2I$ spectrum, and spectra of *g*-$CF_3CF_2CF_2^\bullet$ and *a*-$CF_3CF_2CF_2^\bullet$. The negative peaks were reproduced by inverting the equilibrium spectrum of $CF_3CF_2CF_2I$. New absorption features were recovered by

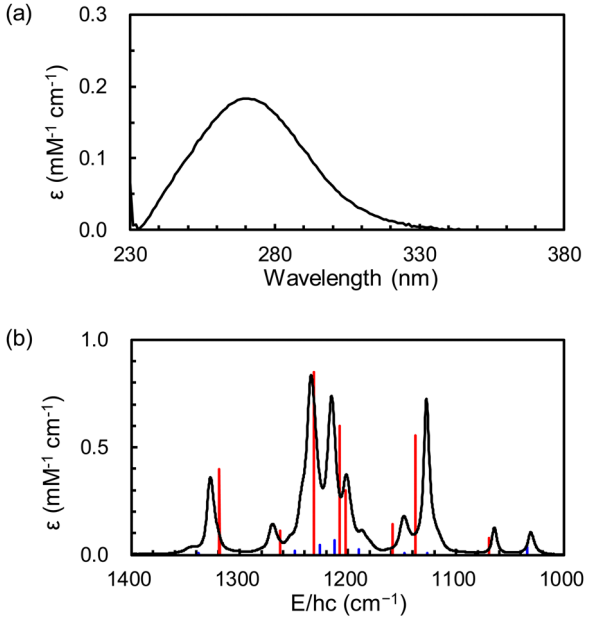

Fig. 4 Equilibrium (a) UV-vis and (b) FTIR spectra of $CF_3CF_2CF_2I$ in CCl_4 solution measured at room temperature. The calculated vibrational spectra of *g*-$CF_3CF_2CF_2I$ (blue) and *a*-$CF_3CF_2CF_2I$ (red) are shown as vertical lines with a scale factor of 0.989.

summing the two spectra assigned to *g*-$CF_3CF_2CF_2^\bullet$ and *a*-$CF_3CF_2CF_2^\bullet$ with the help of the vibrational frequencies calculated by DFT using ωB97XD/aug-cc-pVTZ. The lower panel of Fig. 5 shows that the TRIR spectra are reproduced well by the sum of the three basis spectra shown in the upper panel of Fig. 5.

Time-dependent amplitude changes of the basis spectra for *g*-$CF_3CF_2CF_2^\bullet$ and *a*-$CF_3CF_2CF_2^\bullet$ were obtained from global fitting, as shown in Fig. 6. The amplitude changes demonstrate that the fraction of *a*-$CF_3CF_2CF_2^\bullet$ decreases while that of *g*-$CF_3CF_2CF_2^\bullet$ increases simultaneously, indicating that excess *a*-$CF_3CF_2CF_2^\bullet$ produced upon photodissociation of $CF_3CF_2CF_2I$ rotationally isomerizes into *g*-$CF_3CF_2CF_2^\bullet$. The relative Gibbs free energies of *g*-$CF_3CF_2CF_2I$ (*g*-$CF_3CF_2CF_2^\bullet$) compared to those of *a*-$CF_3CF_2CF_2I$ (*a*-$CF_3CF_2CF_2^\bullet$) were calculated to be 1.83 (0.21) kcal mol^{-1} at 293 K, resulting in equilibrium mole fractions of *a*-$CF_3CF_2CF_2I$ (*a*-$CF_3CF_2CF_2^\bullet$) of 0.92 (0.42). The mole fractions of the rotational isomers for the nascent photoproduct appear similar to those of the reactant, indicating that the rotational conformer of $CF_3CF_2CF_2I$ in CCl_4 mostly dissociates I atoms before rotational isomerization occurs under excitation at 267 nm. In other words, ∼92% of the dissociated radicals are expected to be *a*-$CF_3CF_2CF_2^\bullet$ and, thus, they undergo rotational isomerization to reach the equilibrium mole fraction of 42%.

Time-dependent amplitude changes of the basis spectra for *g*-$CF_3CF_2CF_2^\bullet$ and *a*-$CF_3CF_2CF_2^\bullet$ were well reproduced by the kinetics of rotational isomerization of $CF_3CF_2CF_2^\bullet$ with a time constant of 34 ps. In other words, τ_{rot} = 34 ps around the C–C$^\bullet$ bond of $CF_3CF_2CF_2^\bullet$ in CCl_4 at 293 K. A τ_{rot} of 30 ps was calculated at 293 K using Kramers' theory based on the energies

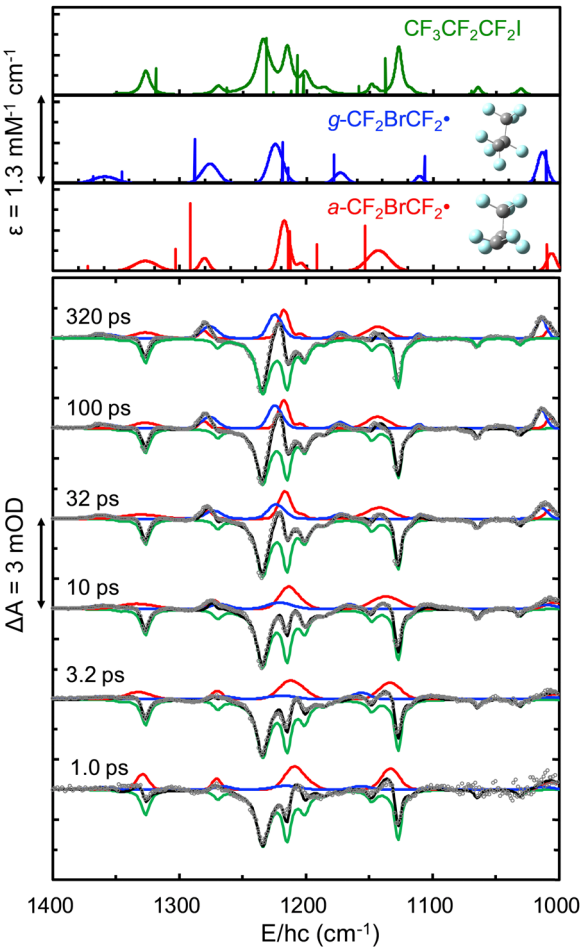

Fig. 5 (Top) Basis spectra used to fit the TRIR spectra for $CF_3CF_2CF_2I$, g-$CF_3CF_2CF_2$•, and a-$CF_3CF_2CF_2$•. The calculated peaks are labeled as vertical lines with a scale factor of 0.989. Also shown are the optimized structures of two CF_2BrCF_2 radicals calculated using DFT with ωB97XD/aug-cc-pVTZ conditions. The gray and light blue spheres represent C and F atoms, respectively. (Bottom) Representative TRIR spectra of $CF_3CF_2CF_2I$ in CCl_4 at 293 K after excitation at 267 nm. The absorbance is given as the optical density (OD), where 1 mOD = 10^{-3} OD. The spectra were decomposed into their basis spectra (color-coded as shown in the top panel). Data (open circles) were well described by the sum of three basis spectra (black lines).

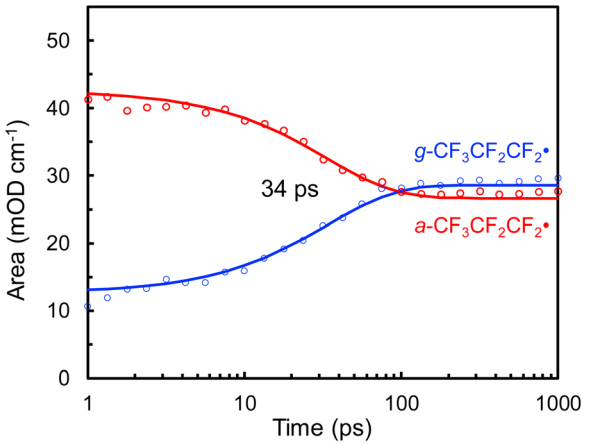

Fig. 6 Time-dependent amplitude changes of the basis spectra of g-$CF_3CF_2CF_2$• and a-$CF_3CF_2CF_2$• obtained by globally fitting TRIR spectra of $CF_3CF_2CF_2I$ in CCl_4 at 293 K after excitation at 267 nm. The amplitude changes (open circles) are well reproduced by the rotational isomerization kinetics with a time constant of 34 ps (solid lines).

and vibrational frequencies calculated by DFT with ωB97XD/aug-cc-pVTZ. The calculated and experimental τ_{rot} values are similar, confirming that Kramers' theory is suitable for calculating τ_{rot} around the C–C bond of ethyl derivatives in solution. We also calculated the τ_{rot} for several ethyl derivatives and ethane derivatives (see Table 3). For example, τ_{rot} = 58 ps for $CH_3CH_2CH_2CH_3$ in CCl_4 at 298 K, which is about 3 times slower than the values obtained by MD simulations of *n*-butane as a model liquid at 292 or 273 K, but slightly faster than the value of 81 ps estimated using κ = 0.75 and the value of the TST.[4] Since all of the MD simulations referenced here used the Ryckaert–Bellemans dihedral angle potential, which has a lower barrier energy than that calculated by DFT,[4,35] a faster rotational time is expected. It would be interesting to determine the τ_{rot} of $CH_3CH_2CH_2CH_3$ in CCl_4 by performing MD simulations using the rotational barrier obtained by the DFT method used here.

A τ_{rot} of 0.64 ns was calculated for CH_2ClCF_2Cl, which can be determined experimentally by 2D IR vibrational echo spectroscopy as the two *gauche*- and *anti*-conformations have distinct C–F stretching modes and the vibrational relaxation time is slow enough to determine τ_{rot}. In a future study, we plan to measure τ_{rot} around the C–C bond of CH_2ClCF_2Cl to compare the experimental value with the calculated one to confirm that the use of Kramers' theory and DFT calculations with ωB97XD/aug-cc-pVTZ estimates τ_{rot} with sufficient accuracy. These findings could be relevant for analyzing the C–C(•) bonds of ethane derivatives as well as ethyl radical derivatives.

Kramers' theory, a classical approach in theoretical reaction dynamics, assumes diffusive barrier crossing and primarily relies on the harmonic approximation of the modes along the reaction coordinate. However, the nascent CF_2BrCF_2• may not be in a fully thermal equilibrium state during the rotation. Despite this, Kramer's theory appears sufficient for calculating a reliable rate constant of rotation along the C–C• bond of CF_2BrCF_2• in solution. The rotational time constant along the C–C(•) bond in organic compounds can be estimated using Kramers' theory combined with DFT calculations.

Conclusion

We measured the temperature- and viscosity-dependent τ_{rot} about the C–C• bond of CF_2BrCF_2• in solution and compared these values with those calculated using Kramers' theory of reaction rates. The rotational energy barriers and vibrational frequencies of the related compounds required for the calculation of the rate constant using Kramers' theory were calculated by DFT using three different functionals (ωB97XD, APFD, and B3LYP) with the aug-cc-pVTZ basis set to identify a reliable and practical computational method without the need for high-level

Table 3 Rotational isomerization time constant (τ_{rot}) calculated using the Kramers' theory for various compounds in CCl_4 at 298 K. Energies and vibrational frequencies of the related compounds were calculated by DFT using ωB97XD/aug-cc-pVTZ. Zero-point corrected energies were used to calculate the rotational energy barrier. The dielectric constant and viscosity of CCl_4 are 2.228[31] and 0.85 mPa s at 298 K,[32] respectively

Compounds	$\frac{\omega_{TS}}{2\pi c}, \frac{\omega_A}{2\pi c}, \frac{\omega_G}{2\pi c}$ (cm^{-1})	ΔE_{TG} (kcal mol^{-1})	ΔE_{TA} (kcal mol^{-1})	κ^A_{KR}, κ^G_{KR}	τ_{rot} (ps)	τ_{GA}, τ_{AG} (ps)
$CF_2BrCF_2^\bullet$	65, 72, 59	2.06	4.40	0.50, 0.46	38	40, 777
$CF_3CF_2CF_2^\bullet$	56, 38, 35	1.89	2.28	0.42, 0.40	26	58, 49
CF_2BrCF_2I	50, 54, 57	5.19	6.30	0.52, 0.52	5583	7202, 24 840
$CH_3CH_2CH_2CH_3$	132, 59, 104	2.63	3.45	0.36, 0.37	58	74, 265
					22[a]	57[a], 37[a]
					21[b]	53[b], 34[b]
					20[c]	47[c], 34[c]
					—	61[d], —
					—	43[e], —
$CH_3CH_2CH^\bullet CH_3$	68, 60, 51	0.07	0.75	0.19, 0.21	3	10, 5
CH_3CH_3	295, 305, 305	2.39	2.39	0.44	4.7[f]	14, —
$CH_3CH_2^\bullet$	99, 111, —	—	−0.11	0.17	0.5[f]	1.5, —
$CF_2ICF_2^\bullet$	65, 73, 57	1.95	5.04	0.57, 0.53	29	30, 2004
CH_2ClCF_2Cl	98, 105, 97	4.39	5.03	0.51, 0.51	645	1122, 1517
CH_2FCH_2NCO	132, 133, 85	3.77	2.68	0.49, 0.50	22	473, 23
					22[g]	—, 43[h]

[a] Obtained by MD simulation of a model liquid at 292 K.[5] [b] Obtained by MD simulation of a model liquid at 292 K.[7] [c] Obtained by MD simulation of a model liquid at 273 K.[9] [d] Obtained by MD simulation of a pure liquid at <292 K.[8] [e] Obtained by MD simulation of $CH_3CH_2CH_2CH_3$ in CCl_4 at 300 K.[9] [f] For CH_3CH_3 and $CH_3CH_2^\bullet$, all conformers are the same, resulting in $\tau_{AG} = \tau_{GA}$ and $\tau_{rot} = \tau_{GA}/3$. [g] Derived from a reported τ_{AG} of 43 ps, obtained from 2D IR vibrational echo chemical exchange spectra measured at room temperature, which was fit assuming $\tau_{AG} = \tau_{GA}$.[3] [h] Experimentally determined at room temperature.[3]

calculations. The τ_{rot} values calculated using Kramers' theory and the DFT results were similar to the experimental ones, and the ωB97XD/aug-cc-pVTZ DFT conditions gave the best results. The τ_{rot} values calculated using Kramers' theory and ωB97XD/aug-cc-pVTZ DFT were further validated by experimentally measuring the τ_{rot} about the C–C$^\bullet$ bond of $CF_3CF_2CF_2^\bullet$ in CCl_4 at 293 K by photodissociating I atoms from $CF_3CF_2CF_2I$ at 267 nm. The findings confirm that reliable τ_{rot} values about the C–C(•) bond of ethyl radical and ethane derivatives in solution can be readily obtained using Kramers' theory and DFT.

Author contributions

S. P. and M. L. designed the experiment; S. P. and J. S. collected time-resolved infrared spectra. S. P., H. Y., J. S., and M. L. analyzed the data. S. P. and M. L. wrote the manuscript. All authors approved the final version of the manuscript.

Data availability

The data supporting the findings of this study are provided within the article and its ESI.†

Conflicts of interest

There are no conflicts of interest to declare.

Acknowledgements

This work was supported by a National Research Foundation of Korea grant funded by the Korean government (NRF-2023R1A2C2004993). S. Park was supported by the LAMP program of the NRF grants funded by the Korean government (RS-2023-00301938). We acknowledge the usage of the Femtosecond Laser System in the PNU Core Research Facilities.

References

1 W. J. Orville-Thomas, *Internal Rotation in Molecules*, John Wiley & Sons, 1974.
2 M. B. Smith and J. March, *March's Advanced Organic Chemistry: Reactions, Mechanisms, and Structure*, John Wiley & Sons, Inc., 6th edn, 2006.
3 J. Zheng, K. Kwak, J. Xie and M. D. Fayer, *Science*, 2006, **313**, 1951–1955.
4 S. Park, J. Shin, H. Yoon and M. Lim, *J. Phys. Chem. Lett.*, 2022, **13**, 11551–11557.
5 D. Brown and J. H. R. Clarke, *J. Chem. Phys.*, 1990, **92**, 3062–3073.
6 D. Chandler, *J. Chem. Phys.*, 1978, **68**, 2959–2970.
7 R. Edberg, D. J. Evans and G. P. Morriss, *J. Chem. Phys.*, 1987, **87**, 5700–5708.
8 J. Ramirez and M. Laso, *J. Chem. Phys.*, 2001, **115**, 7285–7292.
9 R. O. Rosenberg, B. J. Berne and D. Chandler, *Chem. Phys. Lett.*, 1980, **75**, 162–168.
10 T. A. Weber, *J. Chem. Phys.*, 1978, **69**, 2347–2354.
11 H. Eyring, *J. Chem. Phys.*, 1935, **3**, 107.
12 P. Haenggi, P. Talkner and M. Borkovec, *Rev. Mod. Phys.*, 1990, **62**, 251–341.
13 N. E. Henriksen and F. Y. Hansen, *Theories of Molecular Reaction Dynamics: The Microscopic Foundation of Chemical Kinetics*, Oxford University Press, 2008.

14 P. Atkins and J. de Paula, *Atkins' Physical Chemistry*, Oxford University Press, 9th edn, 2009.
15 J. Chandrasekhar, S. F. Smith and W. L. Jorgensen, *J. Am. Chem. Soc.*, 1985, **107**, 154–163.
16 R. F. Grote and J. T. Hynes, *J. Chem. Phys.*, 1980, **73**, 2715–2732.
17 J. Tomasi, B. Mennucci and R. Cammi, *Chem. Rev.*, 2005, **105**, 2999–3094.
18 P. Hamm, R. A. Kaindl and J. Stenger, *Opt. Lett.*, 2000, **25**, 1798–1800.
19 S. Park, J. Shin and M. Lim, *Int. J. Mol. Sci.*, 2023, **24**, 1319.
20 M. J. Frisch, G. W. Trucks, H. B. Schlegel, G. E. Scuseria, M. A. Robb, J. R. Cheeseman, G. Scalmani, V. Barone, G. A. Petersson, H. Nakatsuji, X. Li, M. Caricato, A. V. Marenich, J. Bloino, B. G. Janesko, R. Gomperts, B. Mennucci, H. P. Hratchian, J. V. Ortiz, A. F. Izmaylov, J. L. Sonnenberg, D. Williams-Young, F. Ding, F. Lipparini, F. Egidi, J. Goings, B. Peng, A. Petrone, T. Henderson, D. Ranasinghe, V. G. Zakrzewski, J. Gao, N. Rega, G. Zheng, W. Liang, M. Hada, M. Ehara, K. Toyota, R. Fukuda, J. Hasegawa, M. Ishida, T. Nakajima, Y. Honda, O. Kitao, H. Nakai, T. Vreven, K. Throssell, J. A. Jr., J. E. Peralta, F. Ogliaro, M. J. Bearpark, J. J. Heyd, E. N. Brothers, K. N. Kudin, V. N. Staroverov, T. A. Keith, R. Kobayashi, J. Normand, K. Raghavachari, A. P. Rendell, J. C. Burant, S. S. Iyengar, J. Tomasi, M. Cossi, J. M. Millam, M. Klene, C. Adamo, R. Cammi, J. W. Ochterski, R. L. Martin, K. Morokuma, O. Farkas, J. B. Foresman and D. J. Fox, *Gaussian 16, Revision B.01*, Gaussian, Inc., Wallingford CT, 2016.
21 R. Dennington, T. A. Keith and J. M. Millam, *GaussView, Version 6*, Semichem Inc., Shawnee Mission, KS, 2016.
22 J.-D. Chai and M. Head-Gordon, *J. Chem. Phys.*, 2008, **128**, 084106.
23 J.-D. Chai and M. Head-Gordon, *Phys. Chem. Chem. Phys.*, 2008, **10**, 6615–6620.
24 A. Austin, G. A. Petersson, M. J. Frisch, F. J. Dobek, G. Scalmani and K. Throssell, *J. Chem. Theory Comput.*, 2012, **8**, 4989–5007.
25 A. D. Becke, *J. Chem. Phys.*, 1993, **98**, 5648.
26 F. Jensen, *J. Chem. Theory Comput.*, 2014, **10**, 1074–1085.
27 P. J. Wilson, T. J. Bradley and D. J. Tozer, *J. Chem. Phys.*, 2001, **115**, 9233–9242.
28 G. M. Nathanson, T. K. Minton, S. F. Shane and Y. T. Lee, *J. Chem. Phys.*, 1989, **90**, 6157–6170.
29 M. Rasmusson, A. N. Tarnovsky, T. Pascher, V. Sundstroem and E. Akesson, *J. Phys. Chem. A*, 2002, **106**, 7090–7098.
30 G. Scalmani and M. J. Frisch, *J. Chem. Phys.*, 2010, **132**, 114110.
31 C. Wohlfahrt and M. D. Lechner, *Static Dielectric Constants of Pure Liquids and Binary Liquid Mixtures*, Springer-Verlag Berlin Heidelberg, 1st edn, 2015.
32 Chemical Engineering and Materials Research Information Center, Pure Component Properties, (**https://www.cheric.org/research/kdb/hcprop/cmpsrch.php**).
33 J. M. Bernal-García, A. Guzmán-López, A. Cabrales-Torres, A. Estrada-Baltazar and G. A. Iglesias-Silva, *J. Chem. Eng. Data*, 2008, **53**, 1024–1027.
34 E. Gerck, *J. Chem. Phys.*, 1983, **79**, 311.
35 J. P. Ryckaert and A. Bellemans, *Faraday Discuss. Chem. Soc.*, 1978, **66**, 95–106.

